Uniaxial stress dependence of current-voltage characteristics in GaAs-$Al_xGa_{1-x}As$-GaAs heterojunction barriers

S. S. Lu, K. Lee,[a] and M. I. Nathan
Department of Electrical Engineering, University of Minnesota, 200 Union Street S.E., Minneapolis, Minnesota 55455

M. Heiblum and S. L. Wright
IBM Thomas J. Watson Research Center, Yorktown Heights, New York 10598

(Received 26 April 1989; accepted for publication 17 July 1989)

Current-voltage characteristics of nGaAs-iAl$_x$Ga$_{1-x}$As-nGaAs heterojunction barriers grown on (100) substrates have been measured under uniaxial stress along ⟨100⟩ at 77 K. The results show that thermionic emission current through longitudinal X valleys becomes dominant over Fowler–Nordheim tunneling current through Γ or transverse X valleys, as stress increases. From the stress-dependent thermionic emission current the rate of change with stress of the band-edge energy difference between Γ in GaAs and longitudinal X in AlGaAs is deduced to be 14 ± 2 meV/kbar, which leads to an X-valley shear deformation potential of 9.6 ± 1.8 eV.

Recently, transport properties of electrons across n-doped GaAs–undoped $Al_xGa_{1-x}As$–n-doped GaAs double heterojunction single tunnel barrier have drawn much attention[1,2] due to the extensive effort to develop ultrahigh-speed electron devices using this barrier.[3–5] Depending on the composition x, the Γ, X, and perhaps the L valleys in k space of the AlGaAs layer will be involved in the tunneling. Furthermore, the individual X and L valleys can contribute differently depending on their orientation with respect to the current direction. For tunneling in the ⟨100⟩ direction through X valleys, for example, there are two different orientations, i.e., two longitudinally oriented X valleys (X_l) with high mass $\sim m_0$ (m_0 is the free-electron mass) and four transversely oriented X valleys (X_t) with smaller mass $\sim 0.2m_0$ in the current direction. Although there is evidence that in some cases the latter dominates over the former,[2,6,7] the role of X_l is not clear yet. This is because, while the tunneling mass through X_t is much smaller compared to that through X_l, tunneling through X_l can be favored by momentum conservation perpendicular to the barrier. Even though some theoretical work has been reported on the tunneling through longitudinal valleys,[8,9] as far as we know, there has been no experimental observation of current dominated by tunneling through these valleys.

In this letter, uniaxial stress-dependent current-voltage (I-V) characteristics of nGaAs-iAl$_x$Ga$_{1-x}$As-nGaAs double heterojunction single tunnel barriers are measured. Our stress is compressive and applied longitudinally along the ⟨100⟩ direction perpendicular to the heterojunction barrier by means of a push rod with a lever system.[10] This study relies on the fact that uniaxial stress along ⟨100⟩ can remove the degeneracy of X valleys.[11,12] Thus, when uniaxial stress is applied in the ⟨100⟩ direction, the minimum energy of X_t will increase compared to the valence band, while that of X_l will decrease, enabling us to separate the current components flowing through each valley. The results of our measurement are that we are able to demonstrate the usefulness of uniaxial stress in elucidating the tunneling mechanism in heterojunction barriers. We directly observed the surprising and new result that, for Fowler–Nordheim tunneling, under appropriate conditions, the final state is not the lowest energy valley, but the higher valley favored by effective mass and momentum conservation. For the case of thermionic emission and thermionic field emission, in which thermally activated electrons tunnel through a small barrier, the lowest energy barrier tends to dominate.

Our experiments were done on three n^+GaAs-iAl$_x$Ga$_{1-x}$As-nGaAs heterostructure samples grown by molecular beam epitaxy on (100) n^+GaAs wafers. The characteristics of the layers are summarized in Table I. Buffer layer thickness is about 0.6 μm for all samples. All samples are circular mesas with 2 μm height and 200 μm diameter.

Figure 1(a) shows experimental results for sample A, which has many remarkably interesting features. At first, the I-V characteristic does not change with stress at all at low stress. As we increase the stress, the current at low voltage increases very rapidly, while the current at high voltage remains the same. We attribute this behavior to the crossover of Γ and X_l in AlGaAs. According to the data reported in Ref. 13, the energy of Γ in AlGaAs for $x = 0.32$ sample is lower than that of X by about 70 meV at zero stress. When uniaxial stress is applied in the ⟨100⟩ direction, the Γ minimum in AlGaAs will move almost at the same rate as that in GaAs.[14] In other words,

TABLE I. Characteristics of three n^+GaAs-iAl$_x$Ga$_{1-x}$As-nGaAs heterostructure samples used in our experiment.

Sample i.d.	n^+ top layer doping (10^{18} cm^{-3})	Barrier Aluminum composition x	Barrier Thickness (Å)	Buffer doping (10^{18} cm^{-3})
A	1	0.32	400	1
B	1	0.5	350	0.01
C	1	0.8	400	0.01

[a] Permanent address: Department of Electrical Engineering, Korea Advanced Institute of Science and Technology, Cheongryang, Seoul, Korea.

 0003-6951/89/391336-03$01.00

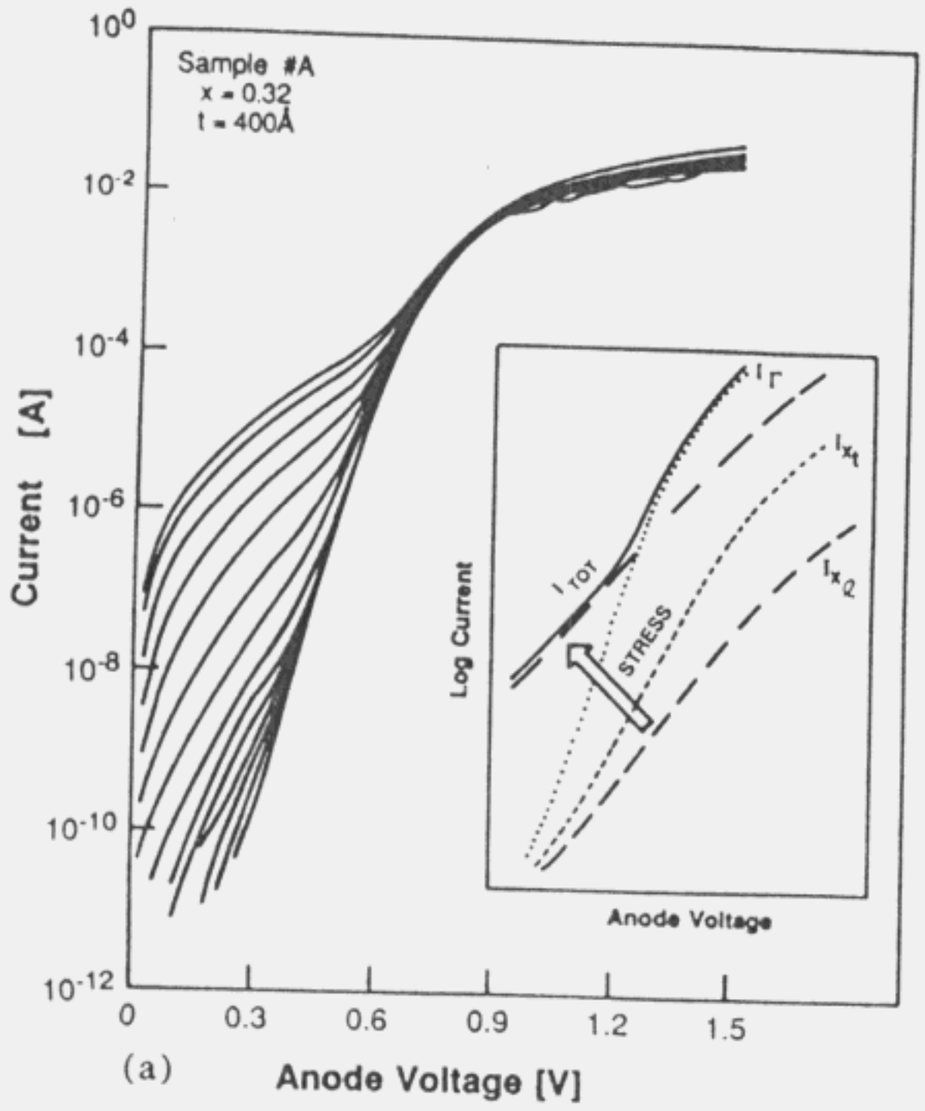

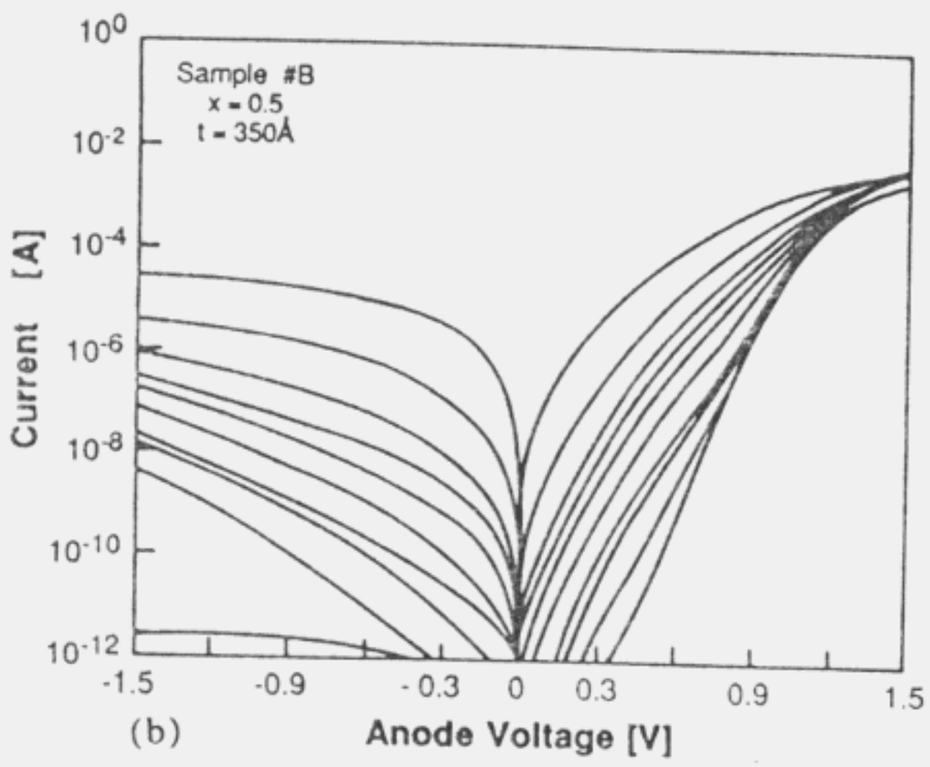

FIG. 1. Measured *I-V* characteristics at 77 K with net weight as a parameter. The stressed area is circular with 200 μm diameter in all cases. (a) *I-V* characteristics of sample A. Bottom curve corresponds to zero to 840*g* and top curve to 3440*g* with 200*g* step. Inset schematically shows the total current (I_{TOT}, solid line) at high stress comprised of three components; current through Γ valley in AlGaAs (I_Γ, dotted line), through X_t (I_{x_t}, dashed line), and through X_l (I_{x_l}, heavy dashed line). Under uniaxial stress along ⟨100⟩, only I_{x_l} increases appreciably. (b) *I-V* characteristics of sample B (bottom, zero; top, 2200*g*; first seven steps, 200*g*; last two steps, 400*g*).

$$\delta(E_1^\Gamma - E_0^\Gamma)/\delta S \approx 0\,, \tag{1}$$

where S is the stress and E_1^Γ and E_0^Γ are the Γ energy minima in AlGaAs and GaAs, respectively. On the other hand, the X-valley minima will move at different rates as follows[11]:

$$\frac{\delta(E_1^{X_l} - E_0^\Gamma)}{\delta S} = \frac{1}{3}\frac{\delta(E_1^X - E_0^\Gamma)}{\delta P} - \frac{2}{3}\Xi_u^X(S_{11} - S_{12})\,, \tag{2}$$

$$\frac{\delta(E_1^{X_t} - E_0^\Gamma)}{\delta S} = \frac{1}{3}\frac{\delta(E_1^X - E_0^\Gamma)}{\delta P} + \frac{1}{3}\Xi_u^X(S_{11} - S_{12})\,. \tag{3}$$

Here P is the hydrostatic pressure; Ξ_u^X, the shear deformation potential of X valleys in AlGaAs; S_{11} and S_{12}, components of the compliance tensor; E_1^X, the energy minima of X valleys under hydrostatic pressure; $E_1^{X_l}$ and $E_1^{X_t}$, the energy minima of X_l and X_t, respectively. The movement of the minimum valley energies under uniaxial stress governed by Eqs. (2) and (3) is illustrated in Fig. 2.

Because E_1^X is higher than E_1^Γ for sample A at zero stress, we can see from Fig. 2(a) and Eq. (1) that the minimum barrier is determined by the difference between Γ in AlGaAs and Γ in GaAs and remains constant for the stress smaller than the critical stress, S_c. This explains why the *I-V* characteristics do not change at all at low stress in Fig. 1(a). However, as the stress increases further, $E_1^{X_l}$ becomes smaller than E_1^Γ. When this happens, thermionic emission (TE) through X_l is dominant over TE and thermionic field emission (TFE) through Γ. But at high bias Fowler–Nordheim tunneling (FN) through Γ is still dominant over TE through X_l. This is because the tunneling mass of X_l is much larger than that of Γ[2]. At zero stress all currents are through Γ in AlGaAs. But as stress increases, TE through X_l increases rapidly and becomes dominant, while FN through Γ stays the same. This is consistent with Eqs. (1) and (2) and Fig. 2 and is illustrated in the inset of Fig. 1(a), which shows the three current components through each valley and the increase of the current through X_l under uniaxial stress.

Figure 1(b) shows *I-V* characteristics with stress as a parameter for sample B. Sample C shows similar characteristics with higher current density. Because these samples are doped asymmetrically, we observe TE at reverse bias and TE, TFE, and FN at forward bias.

The stress-dependent current characteristics at fixed voltages for our samples are shown in Fig. 3. The major difference of the stress dependence of samples B and C from that of A is that the current starts to increase rapidly as soon

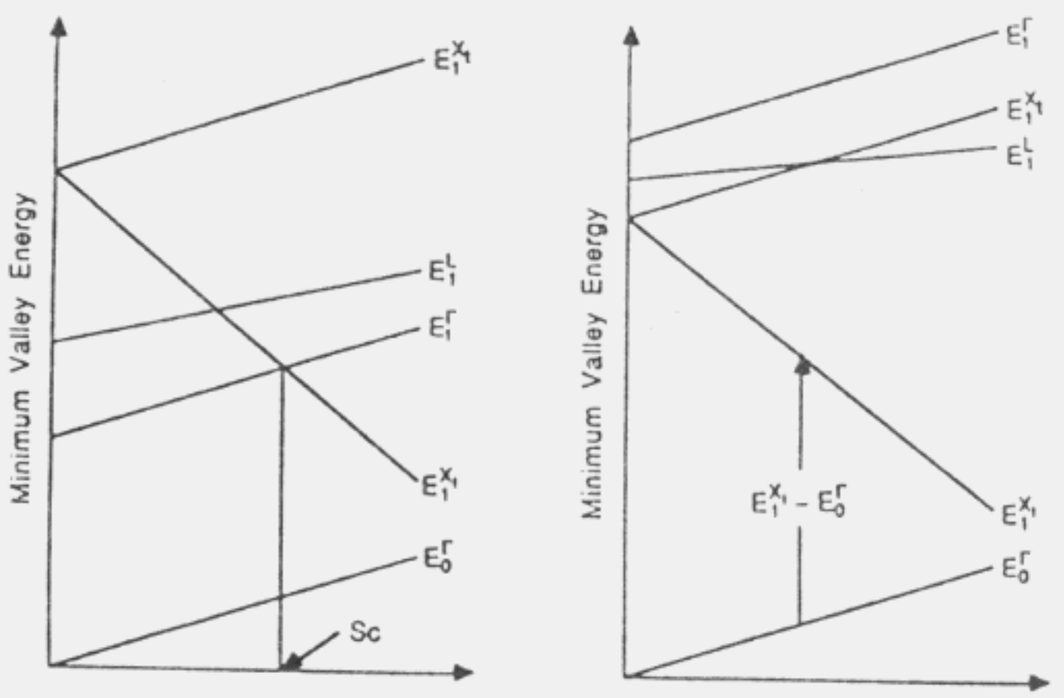

FIG. 2. Schematic illustration of the movement of the minimum valley energies relative to the average valence band under longitudinal stress along ⟨100⟩, for GaAs and AlGaAs conduction bands. (a) is for direct-gap AlGaAs with low x, and (b) for indirect-gap AlGaAs with high x. S_c is the critical stress for the energy crossover between E_1^Γ and $E_1^{X_l}$ of direct-gap AlGaAs. See text for the definition of symbols.

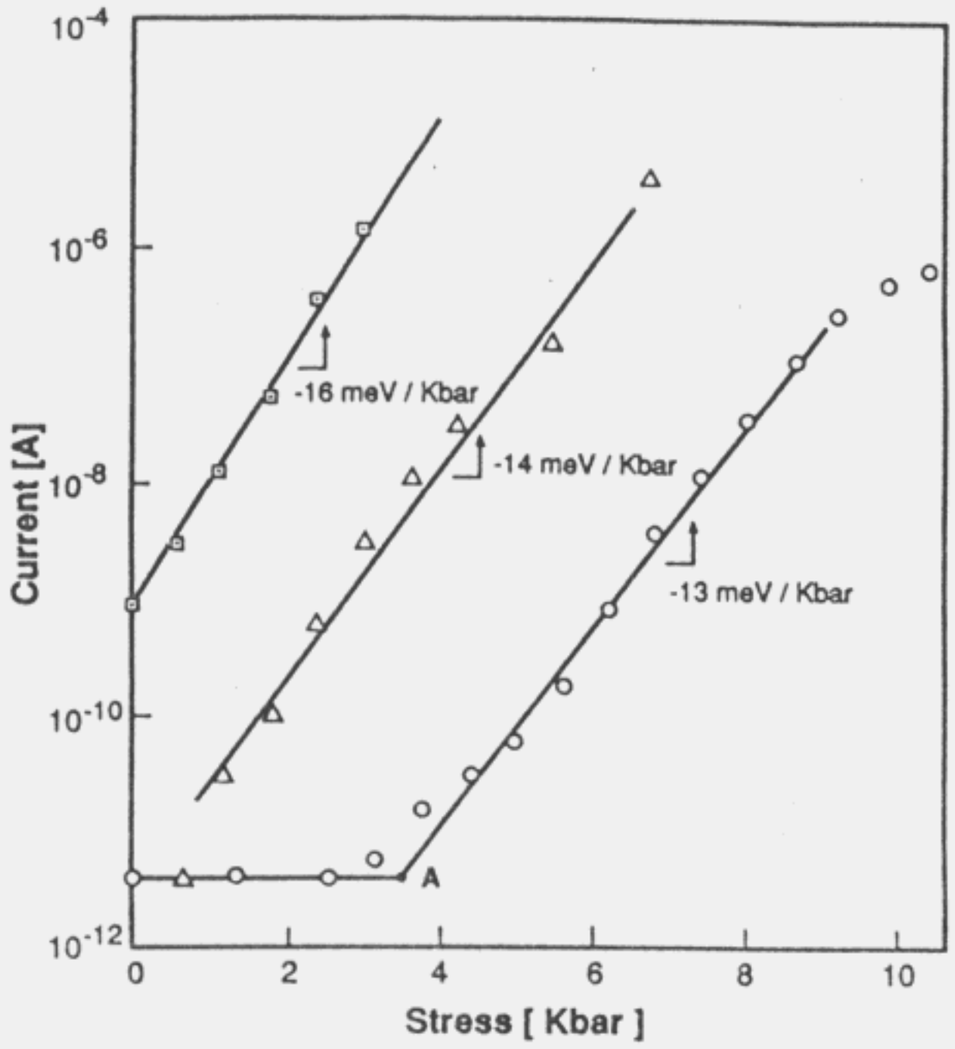

FIG. 3. Log of current vs stress at fixed voltages. Open circles are for sample A measured at 0.25 V. Open triangles for sample B and open squares for sample C measured at 0.3 V, respectively. Point marked as *A* is the current crossover critical stress point (3.6 kbar) for sample A.

as stress is applied. This agrees with the hydrostatic pressure results reported earlier[6] and confirms that the X valleys are the lowest conduction band at zero stress. As stated earlier,[15] in TE and a wide range of TFE regimes, the current is proportional to $\exp(-\phi_B/kT)$ at a fixed voltage, where kT is the thermal energy and ϕ_B is the barrier height. ϕ_B is the difference between E_1^Γ (or E_1^X) and the Fermi energy in GaAs. The Fermi energy in GaAs in reference to E_0^Γ is only dependent on the electric field at the GaAs/AlGaAs interface. Thus, at a fixed bias (field), $\delta\phi_B/\delta S$ is the same as either $\delta(E_1^\Gamma - E_0^\Gamma)/\delta S$ or $\delta(E_1^{X_l} - E_0^\Gamma)/\delta S$. The rates of the barrier lowering $\delta(E_1^{X_l} - E_0^\Gamma)/\delta S$ calculated from the slopes in Fig. 3 are -13 meV/kbar, -14 meV/kbar, and -16 meV/kbar, for samples A, B, and C, respectively. The fact that these values are very close to each other indicates the stresses are fairly uniform, if we assume constant Ξ_u^X in AlGaAs independent of x.

If we insert the measured value of 14 ± 2 meV/kbar as $\delta(E_1^{X_l} - E_0^\Gamma)/\delta S$ into Eq. (2) and use $\delta(E_1^X - E_0^\Gamma)/\delta P = -12.0$ meV/kbar,[14,16] $S_{11} = 1.17 \times 10^{-6}$ bar^{-1}, and $S_{12} = -0.37 \times 10^{-6}$ bar^{-1} for GaAs,[17] we find the X-valley shear deformation potential to be 9.6 ± 1.8 eV. This value is closer to Si (8.6 eV) than GaP (6.9 eV), but much less than previously reported values as suspected in Ref. 18. As far as we know, our result of 9.6 ± 1.8 eV is the most accurately measured values of X-valley shear deformation potential to date, which, however, may depend on the aluminum composition x.

The measured value of critical stress from the current crossover for sample A in Fig. 3 is 3.6 kbar. This agrees fairly well with the critical stress of 5 kbar for the energy crossover of Γ and X_l in AlGaAs, which is obtained from the difference between $E_1^X - E_1^\Gamma$ (70 meV) at zero stress divided by 14 meV/kbar. However, exact comparison of the critical stress value obtained from current crossover with that from energy crossover is difficult due to many unknown parameters contributing current, such as tunneling probability, effective Richardson constant, etc.

When we concentrate on the high forward bias region in Fig. 1(b), we can see that the current does not change much, which is very similar to Fig. 1(a). This is because at high forward bias, FN through X_t dominates over the TE through X_l, and X_t barrier height remains almost constant with uniaxial stress. This coincides with Eq. (3), whose numerical value is very close to zero (1 meV/kbar), implying our stress is uniaxial, even though an additional hydrostatic pressure component may be expected in this kind of experiment.[19] If there is hydrostatic pressure, the current at large forward bias also should increase very rapidly.[6]

Details of our experimental results and comparison with theory will be reported elsewhere.[20]

In summary, current-voltage characteristics of nGaAs-iAl$_x$Ga$_{1-x}$As-nGaAs heterojunction barriers grown on (100) substrates have been measured under uniaxial stress along ⟨100⟩. They show that TE through longitudinal X valleys becomes dominant over FN through either Γ or transverse X valleys, as stress increases, while the latter is almost independent of stress level in the range investigated in this work. From the stress-dependent thermionic emission current the rate of change with stress of the band-edge energy difference between Γ in GaAs and longitudinal X valleys in AlGaAs is deduced to be 14 ± 2 meV/kbar, which leads to an X-valley shear deformation potential of 9.6 ± 1.8 eV. This is believed to be the most accurate value measured to date.

Support from NSF through contract No. NSF/ECS-8803928 and IBM is gratefully acknowledged. We also would like to thank F. O. Williamson and S. Gilbert for useful discussions.

[1] D. Delagebeaudeuf, P. Delescluse, P. Etienne, J. Massies, M. Laviron, J. Chaplart, and T. Linh, Electron. Lett. **18**, 85 (1982).
[2] P. M. Solomon, S. L. Wright, and C. Lanza, Superlatt. Microstruct. **2**, 521 (1986).
[3] L. L. Chang, L. Esaki, and R. Tsu, Appl. Phys. Lett. **24**, 593 (1974).
[4] M. Heiblum, D. C. Thomas, C. M. Knoedler, and M. I. Nathan, Appl. Phys. Lett. **47**, 1105 (1985).
[5] P. M. Solomon, C. M. Knoedler, and S. L. Wright, IEEE Electron Device Lett. **EDL-5**, 379 (1984).
[6] E. E. Mendez, E. Calleja, and W. I. Wang, Phys. Rev. B **34**, 6026 (1986).
[7] E. E. Mendez, E. Calleja, and W. I. Wang, Appl. Phys. Lett. **53**, 977 (1988).
[8] P. J. Price, Surf. Sci. **196**, 394 (1988).
[9] H. Akera, S. Wakahara, and T. Ando, Surf. Sci. **196**, 694 (1988).
[10] J. E. Smith, J. C. McGroddy, and M. I. Nathan, Phys. Rev. **186**, 727 (1969).
[11] C. Pickering and A. R. Adams, J. Phys. C **10**, 3115 (1977).
[12] P. M. Solomon, S. L. Wright, and D. La Tulipe, Appl. Phys. Lett. **49**, 1453 (1986).
[13] J. Batey and S. L. Wright, J. Appl. Phys. **59**, 200 (1986).
[14] U. Venkateswaran, M. Chandrasekhar, H. R. Chandrasekhar, B. A. Vojak, F. A. Chambers, and J. M. Meese, Phys. Rev. B **33**, 8416 (1986).
[15] E. L. Murphy and R. H. Good, Jr., Phys. Rev. **102**, 1464 (1956).
[16] D. J. Wolford and J. A. Bradley, Solid State Commun. **53**, 1069 (1985).
[17] S. Adachi, J. Appl. Phys. **58**, R1 (1985).
[18] D. E. Aspnes and M. Cardona, Phys. Rev. B **17**, 741 (1978).
[19] M. Cuevas and H. Fritzsche, Phys. Rev. A **137**, 1847 (1965).
[20] S. S. Lu, K. R. Lee, K. H. Lee, M. I. Nathan, M. Heiblum, and S. L. Wright (unpublished).